Direct method of extracting broadband complex refractive index from spectrophotometric measurements: an application to polydimethylsiloxane for passive radiative cooling

Braden Czapla[a,*], **Leonard Hanssen**[b]
[a]Sensor Science Division, National Institute of Standards and Technology, 100 Bureau Drive, Gaithersburg, MD 20899, USA

Abstract. We describe an algorithm to extract the complex refractive index of a material from broadband reflectance and transmittance measurements taken by spectrophotometers. The algorithm combines Kramers-Kronig analysis with an inversion of Fresnel's equations to provide a direct method of solving for the refractive index which is accurate, even for weakly absorbing materials, and easily applicable to radiative heat transfer calculations. The algorithm is validated by extracting the complex refractive index of polydimethylsiloxane between 0.25 μm and 100 μm and comparing against existing literature. We also discuss the importance of broadband optical properties to passive radiative cooling and details of the uncertainty analysis of the algorithm.

Keywords: refractive index, Kramers-Kronig, spectrophotometry, polydimethylsiloxane.

*Braden Czapla, braden.czapla@nist.gov

1 Introduction

Polydimethylsiloxane (PDMS) is a silicone elastomer with demonstrated uses in numerous optical technologies such as lenses,[1,2] mirrors,[3] waveguides,[4,5] and filters.[6] These technologies have primarily focused on applications involving visible light, and are enabled by the well studied optical properties of PDMS in the visible portion of the electromagnetic spectrum. In recent years PDMS has emerged as a promising material in passive radiative cooling (PRC) technology,[7–9] a different class of optical technology which seeks to engineer the emittance profile in order to optimally radiate heat at select wavelengths.

PRC leverages devices which selectively emit thermal energy within the atmosphere's infrared transmission window, between approximately 8 μm and 13 μm.[10,11] Due to the broadband nature of radiative heat transfer, a complete simulation of daytime PRC requires knowledge of extremely spectrally broad optical properties, ranging from the shortest wavelengths in the solar spectrum to

the long wavelength tail of a blackbody spectrum at terrestrial temperatures. Unfortunately, most works in the literature do not span sufficiently large spectral ranges (see Fig. 3 and Sec. 4).

The goal of this work is threefold: first, to report a direct method of analyzing spectrophotometric measurements to extract the complex refractive index of a material over a broad spectral range; second, to validate the method against other works in the literature for a material used in PRC technology (in this case, PDMS); and third, to demonstrate the broad spectral data the method can provide is both convenient to obtain and necessary to use in radiative cooling calculations. The structure of this work is as follows. In Sec. 2, we will outline an algorithm to compute complex refractive index using direct methods. We will cover a method of inverting measured reflectance and transmittance and a method of applying Kramers-Kronig analysis to first surface reflectance data. These two methods combine to form Algorithm 1, which we use in this work. Then in Sec. 3 we will detail the fabrication and measurement of PDMS samples, as well as compare the resulting optical properties to existing works in the literature. Finally, in Sec. 4 we demonstrate that the broadband optical properties, such as those determined in this work, are necessary to accurately compute passive radiative cooling performance.

2 Direct Determination of Optical Constants

Throughout this work, we will define the complex refractive index, $\widetilde{n}$, as $\widetilde{n} = n + i\kappa$ where the real part, n, is commonly referred to as the refractive index and the imaginary part, κ, is the extinction coefficient. A number of methods exist for determining the complex refractive index from measurements of reflectance and/or transmittance.[12–20] Most attractive for their simplicity are direct methods, i.e., those which may be written $\widetilde{n} = f(R, T)$, where R and T are measured values of reflectance and transmittance. The function f varies from method to method but is a known

function of R, T, and perhaps other easily measurable variables. Many direct methods involve inverting Fresnel equations, but they are often extremely sensitive to noise in the measurands.[21] In this work, we will utilize two direct methods which are less susceptible to measurement noise: an analytical solution recently put forth by Nichelatti[22] and the Kramers-Kronig relations.[23–28]

2.1 *Nichelatti's Method*

Nichelatti examined the case of a thick slab of material with two smooth, parallel faces (see Fig. 1(A) for a schematic).[22] The material of interest, labeled 2, has thickness h and is embedded between two regions labeled 1 and 3. For the purposes of this work, regions 1 and 3 will be taken as vacuum. A ray of light, depicted by an arrow, impinges on the interface between regions 1 and 2. Subsequent reflections and transmissions are shown by the various daughter rays. If the initial ray is taken to have unity intensity, then the first surface reflectance is shown as R_{12}. The reflectance including all contributions from internal reflections is shown as R_{123}. Similarly, the total transmittance taking into account all internal reflections is shown as T_{123}.

Nichelatti determined a direct method of inverting Fresnel's equations for reflectance and transmittance to extract the complex refractive index. The solution is valid for thick slabs (i.e., those in which the multiple reflections of light between the parallel faces add incoherently). The key results of Nichelatti's work are

$$\kappa = \frac{\lambda}{4\pi h} \ln\left(\frac{R_{12}T_{123}}{R_{123} - R_{12}}\right) \tag{1}$$

$$n = \frac{1+R_{12}}{1-R_{12}} + \sqrt{\left(\frac{1+R_{12}}{1-R_{12}}\right)^2 - 1 - \kappa^2}\,, \tag{2}$$

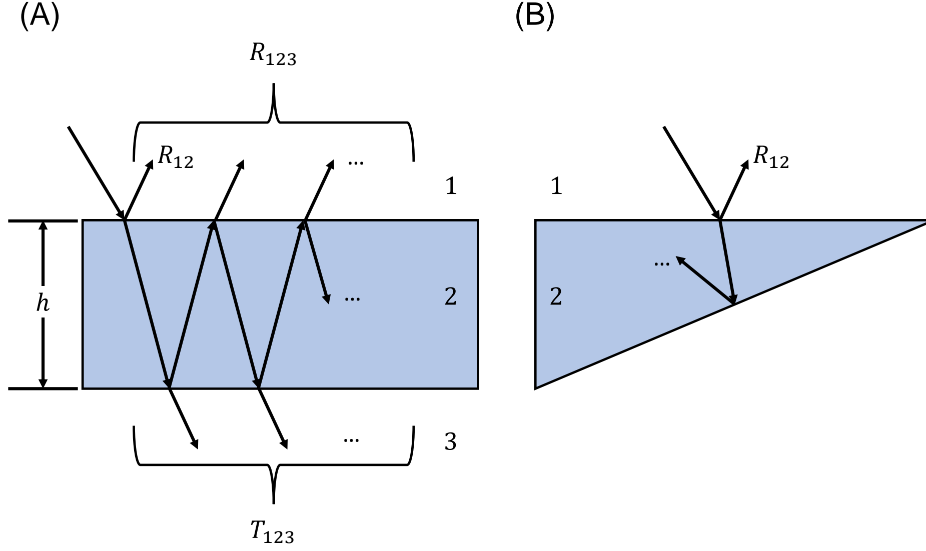

Fig 1 Schematic of measurement geometries. (A) Thick slab of material with thickness h, labelled 2, surrounded my materials 1 and 3. First surface (R_{12}) and total (R_{123}) reflectance are depicted schematically with total transmittance (T_{123}). (B) Wedge of material 2 surrounded by material 1. First surface (R_{12}) reflectance is depicted schematically.

where

$$R_{12} = \frac{2 + T_{123}^2 - (1 - R_{123})^2 - \sqrt{(2 + T_{123}^2 - (1 - R_{123})^2)^2 - 4R_{123}(2 - R_{123})}}{2(2 - R_{123})} \tag{3}$$

and λ is the wavelength. Though not explicitly written here, it is important to note that n, κ, R_{123}, T_{123}, and R_{12} are all functions of λ. Following Nichelatti's methodology, we may also compute R_{123} when only R_{12} and T_{123} are known. Doing so, we get

$$R_{123} = \frac{(R_{12}^2 + 2R_{12} - 1) + \sqrt{(2R_{12}T_{123})^2 + (1 - R_{12})^4}}{2R_{12}} . \tag{4}$$

Explicit formulas for the propagation of experimental uncertainty in Eqs. (1)-(4) are given in Appendix A.

2.2 *Kramers-Kronig Analysis*

Kramers-Kronig analysis is a mathematical technique which takes advantage of the link between the real and imaginary parts of certain analytic functions. The theory, application, and limitations of Kramers-Kronig analysis have been documented thoroughly by various researchers.[23–34] In this work, we will apply Kramers-Kronig analysis to the Fresnel reflection coefficient. At normal incidence, the Fresnel reflection coefficient is related to both R_{12} and $\widetilde{n}$ by

$$r = \sqrt{R_{12}} \exp{(i\delta)} = \frac{\widetilde{n} - 1}{\widetilde{n} + 1}\,, \tag{5}$$

where δ is the phase angle of r. Applying Kramers-Kronig analysis to Eq. (5), we get

$$\delta(\omega) = \frac{-\omega}{\pi} \mathcal{P} \int_0^\infty \frac{\ln{(R_{12}(\omega'))}}{\omega'^2 - \omega^2} d\omega'\,, \tag{6}$$

where ω' is an arbitrary integration variable, $\omega = 2\pi c/\lambda$ is the angular frequency, c is the speed of light in vacuum, and $\mathcal{P}$ indicates the Cauchy principal value. Equation (6) has two important characteristics to note at this time. First, the value of the integrand is not finite for $\omega' = \omega$. Indeed, that is exactly why we must take the Cauchy principal value of the integral. Second, the value of the phase at any single frequency is impacted by the value of reflectance at all frequencies. To evaluate Eq. (6), for an arbitrary sample, even over a finite range, we would need to measure the value of R_{12} at every frequency.

To overcome these two challenges, we draw on innovations from past works. First, we use an integral which evaluates to the same value but has an integrand which is always finite. The

alternative integral has previously been described by Yamamoto and Masui[35] and is given by

$$\delta(\omega) = \frac{-\omega}{\pi} \int_0^\infty \frac{\ln\left(R_{12}(\omega')\right) - \ln\left(R_{12}(\omega)\right)}{\omega'^2 - \omega^2} d\omega' \,. \tag{7}$$

Second, we apply a technique innovated by Roessler[32–34] to address the finite measurement range of their data. Many past works have used extrapolation procedures to artificially extend the range of their data, such as assuming the value of R_{12} is constant outside the measured range[36] or fitting a model to the ends of the measured data and extrapolating it outward.[37–40] Roessler's technique, however, requires only data within the measurement range. Although the integral for δ used by Roessler was not identical to Eq. (7), their technique may be applied to Eq. (7) as well. Roessler broke the integral into three parts and treated each separately. Doing so, we get

$$\delta(\omega) = \alpha(\omega) + \beta(\omega) + \gamma(\omega) \,, \tag{8}$$

where

$$\alpha(\omega) = \frac{-\omega}{\pi} \int_0^{\omega_{\text{lower}}} \frac{\ln\left(R_{12}(\omega')\right) - \ln\left(R_{12}(\omega)\right)}{\omega'^2 - \omega^2} d\omega' \tag{9}$$

$$\beta(\omega) = \frac{-\omega}{\pi} \int_{\omega_{\text{lower}}}^{\omega_{\text{upper}}} \frac{\ln\left(R_{12}(\omega')\right) - \ln\left(R_{12}(\omega)\right)}{\omega'^2 - \omega^2} d\omega' \tag{10}$$

$$\gamma(\omega) = \frac{-\omega}{\pi} \int_{\omega_{\text{upper}}}^{\infty} \frac{\ln\left(R_{12}(\omega')\right) - \ln\left(R_{12}(\omega)\right)}{\omega'^2 - \omega^2} d\omega' \tag{11}$$

and ω_{upper} and ω_{lower} are the upper and lower frequency bounds of the experimental data, respectively. Equation (10) may be evaluated directly from the experimental data using numerical

integration. Integrating by parts, we evaluate to Eq. (9) and (11) to get

$$\alpha(\omega) = \left[C_\alpha(\omega) + \frac{\ln\left[R_{12}(\omega)\right]}{2\pi} \right] \ln\left(\frac{\omega - \omega_{\text{lower}}}{\omega + \omega_{\text{lower}}} \right) \tag{12}$$

$$\gamma(\omega) = \left[C_\gamma(\omega) - \frac{\ln\left[R_{12}(\omega)\right]}{2\pi} \right] \ln\left(\frac{\omega_{\text{upper}} - \omega}{\omega_{\text{upper}} + \omega} \right), \tag{13}$$

where $C_\alpha(\omega)$ and $C_\gamma(\omega)$ are weakly varying functions within $[\omega_{\text{lower}}, \omega_{\text{upper}}]$.

By approximating $C_\alpha(\omega)$ and $C_\gamma(\omega)$ as constant within the measurement range, the problem of needing information from all frequencies outside the measurement range is reduced to a problem of needing the value of the phase of r at two frequencies within the measurement range. With that information, we may solve for C_α and C_γ directly. For any sample which transmits at two frequencies and meets the assumptions of the method, we may apply Nichelatti's method to obtain the values of n and κ and thus obtain δ at those two frequencies from Eq. (5).

2.3 Numerical Algorithm

In this work, we propose the Algorithm 1 for measuring the complex refractive index.

3 Refractive Index of PDMS

3.1 Sample Fabrication and Measurement

PDMS was prepared using a SYLGARD 184 Silicone Elastomer Kit.[1] The pre-polymer base and curing agent were combined in a 10-to-1 ratio by weight and mixed vigorously by hand. Next, portions of the uncured PDMS mixture were poured into three separate polystyrene Petri dishes which served as molds. The remaining uncured PDMS was poured into a wedge-shaped mold with

[1] Certain commercial equipment, instruments, or materials are identified in this paper in order to specify the experimental procedure adequately. Such identification is not intended to imply recommendation or endorsement by NIST, nor is it intended to imply that the materials or equipment identified are necessarily the best available for the purpose.

Algorithm 1 Refractive index extraction algorithm

1. Confirm your samples and instruments are suitable for this method. The materials should have isotropic optical properties. Surfaces should be smooth, specular reflectors. Samples used to measure R_{12} should be non-transmitting or have back surfaces which will reject multiply-reflected light from re-entering the path of the measured light. Samples used to measure R_{123} and/or T_{123} should have two, parallel planar surfaces. They should have at least two transmission bands which enclose the portion of the spectrum being investigated with Kramers-Kronig analysis. The transmission bands should be fairly broad so that the edges of the spectrum being investigated with Kramers-Kronig analysis are redundantly analyzable with Nichelatti's method. The instruments used to measure R_{123} and/or T_{123} must be able to capture all significant internal multiple reflections. Their spectral resolutions, along with thicknesses of samples, must together result in measurements of incoherently adding internal reflections (see Chapter 7 of Ref. 41).

2. Measure two of the three following quantities over as broad of a spectral range as is feasible: R_{12}, R_{123} and T_{123}.

3. Use Eq. (3) or (4) to compute the third unknown quantity.

4. Apply Nichelatti's method to directly solve for n and κ at all frequencies for which the value of T_{123} is statistically distinguishable from zero, as determined by the uncertainty of the measurement.

5. Compute the phase of r using n and κ at two frequencies enclosing the portion of spectrum which T_{123} is statistically equivalent to zero.

6. Compute $\beta(\omega)$ using Eq. (10) and numerical integration.

7. Solve for C_α and C_γ using Eqs. (8), (10), (12), (13), and the two known values of phase.

8. Compute δ for all values of frequency. Use Eq. (5) to solve for $\widetilde{n}$.

9. For any frequency for which the value of n and κ has been computed redundantly, choose the value with a smaller uncertainty. In many cases, this tends to mean choosing values of κ from Nichelatti's method and values of n from Kramers-Kronig analysis. See Appendix A for discussion of uncertainty for each method.

a smooth back surface. The PDMS in the Petri dishes and wedge-shaped mold were allowed to cure at ambient temperatures for approximately 48 h, at which point they were removed from their molds. The PDMS in the polystrene Petri dishes cured into slabs with smooth parallel sides (see Fig. 1(A)). Those three samples henceforth will be referred to as Samples 1, 2, and 3 and they had thicknesses of (1.68 $\pm$ 0.02) mm, (0.30 $\pm$ 0.02) mm and (0.11 $\pm$ 0.02) mm, respectively ($k = 2$ expanded uncertainty), respectively. The PDMS in the wedge-shaped mold cured into a PDMS wedge (see Fig. 1(B)).

The samples were characterized on three separate measurement systems in the Sensor Science Division at the National Institute of Standards and Technology. The reflectance (R_{123}) and transmittance (T_{123}) of Samples 1, 2, and 3 were measured using the NIST transfer spectrophotometer. The NIST transfer spectrophotometer is a commercial dispersive spectrophotometer which measures between $0.25\,\mu\mathrm{m}$ and $2.5\,\mu\mathrm{m}$. The measurements were taken using a sintered polytetrafluoroethylene (PTFE) integrating sphere accessory.

The samples were also measured in the NIST Fourier transform infrared spectrophotometry facility using two Fourier transform infrared spectrophotometers. A custom Fourier transform infrared spectrophotometer system equipped with an integrating sphere[42–46] measured the reflectance (R_{123}) and transmittance (T_{123}) of Samples 1, 2, and 3 between approximately $2\,\mu\mathrm{m}$ and $18\,\mu\mathrm{m}$. A commercial Fourier transform infrared spectrophotometer capable of making measurements under vacuum measured the reflectance of the wedged sample (R_{12}) and the transmittance (T_{123}) of Samples 1, 2, and 3 between approximately $0.8\,\mu\mathrm{m}$ and $100\,\mu\mathrm{m}$. The reflectance of the wedge was measured using a commercial "V/W" absolute reflection accessory. The accessory was used in a relative mode by fixing it in the "W" position and placing a gold mirror on the sample position such that light would reflect once off the PDMS wedge and once off the gold mirror. The PDMS

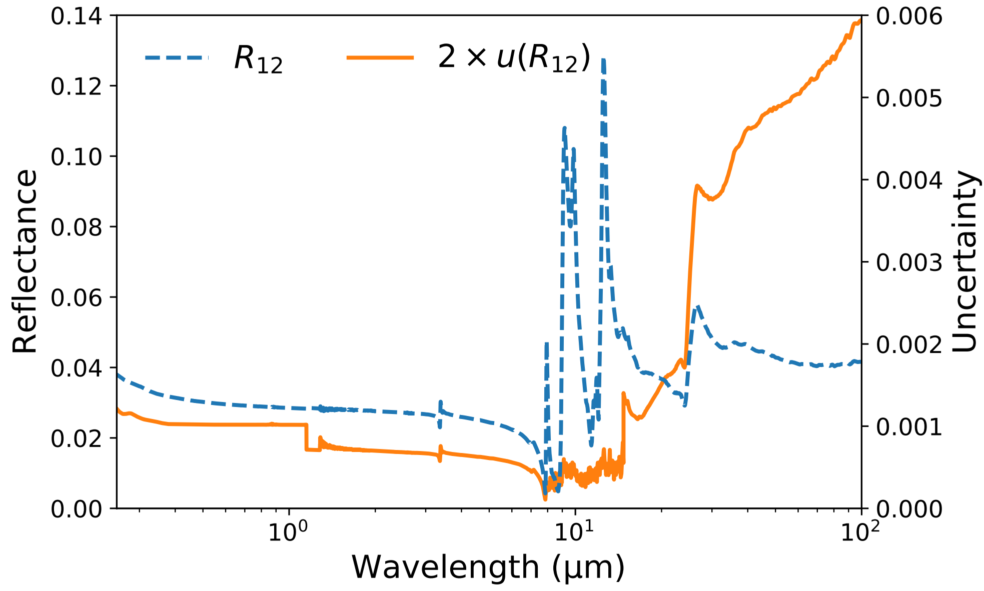

Fig 2 First surface reflectance of PDMS as a function of wavelength and $k = 2$ expanded uncertainty.

wedge was then replaced by a reference mirror to take a relative measurement. This was done due to the relatively low level of reflectance of PDMS. The angle of the back surface of the wedge was determined such that no light which reflected off the back surface could make it back into the path of the light reflected off the first surface.

The broadband spectrum of R_{12} is shown in Fig. 2. The spectrum was formed by extending the data measured from the wedge-shaped sample with values of R_{12} computed from Eq. 3 and the measured values of R_{123} and T_{123} on the NIST transfer spectrophotometer. Also shown is the $k = 2$ expanded uncertainty of R_{12}. The apparent discontinuities in the uncertainty result from merging data from the different instruments and different combinations of beamsplitters, detectors, and sources within the Fourier-transform instrument.

3.2 *Comparison to Literature*

The spectrum of R_{12} shown in Fig. 2 was then used as an input to the Kramers-Kronig algorithm. As discussed in Sec. 2.2, the algorithm also requires known values of the complex refractive at two wavelengths. Equations (1)-(4) were used with measured values of reflectance and transmittance (see Fig. 5) to obtain $\widetilde{n} = (1.390 \pm 0.005) + i(0.0003458 \pm 0.0000041)$ and $\widetilde{n} = (1.508 \pm 0.010) + i(0.008327 \pm 0.00010)$ ($k = 2$) at $\lambda = 3.03\,\mu\text{m}$ and $61.72\,\mu\text{m}$, respectively.

Applying the algorithm, we get the desired values of n and κ between $0.25\,\mu\text{m}$ and $100\,\mu\text{m}$. Data from key intermediate steps of the algorithm can be seen in App. B. The values and the $k = 2$ expanded uncertainties on the values are shown in Fig. 3. Also plotted are the results of numerous other works which measured PDMS in spectral ranges which overlap the present work.[4,47–57] Qualitatively, the results of this work match well to most existing works. There are exceptions, however. The values of n from Refs. 49 and 54 are both visibly higher than the present work and other works in the literature. Values of κ all vary significantly below $2\,\mu\text{m}$. The present work is unable to determine κ between approximately $0.5\,\mu\text{m}$ and $0.6\,\mu\text{m}$. This is due to the extremely weak absorption at those wavelengths. While a thicker sample could be used to better discern κ, special care needs to be taken to either fully capture or exclude internal reflections.

4 Application to Radiative Cooling Calculations

To demonstrate the utility of the measured complex refractive index data, we will examine the emissive power (per unit area) of a radiative cooler over a hemisphere, P_{emit}. This quantity is the sole term in typical passive radiative cooling calculations which depends only on the optical

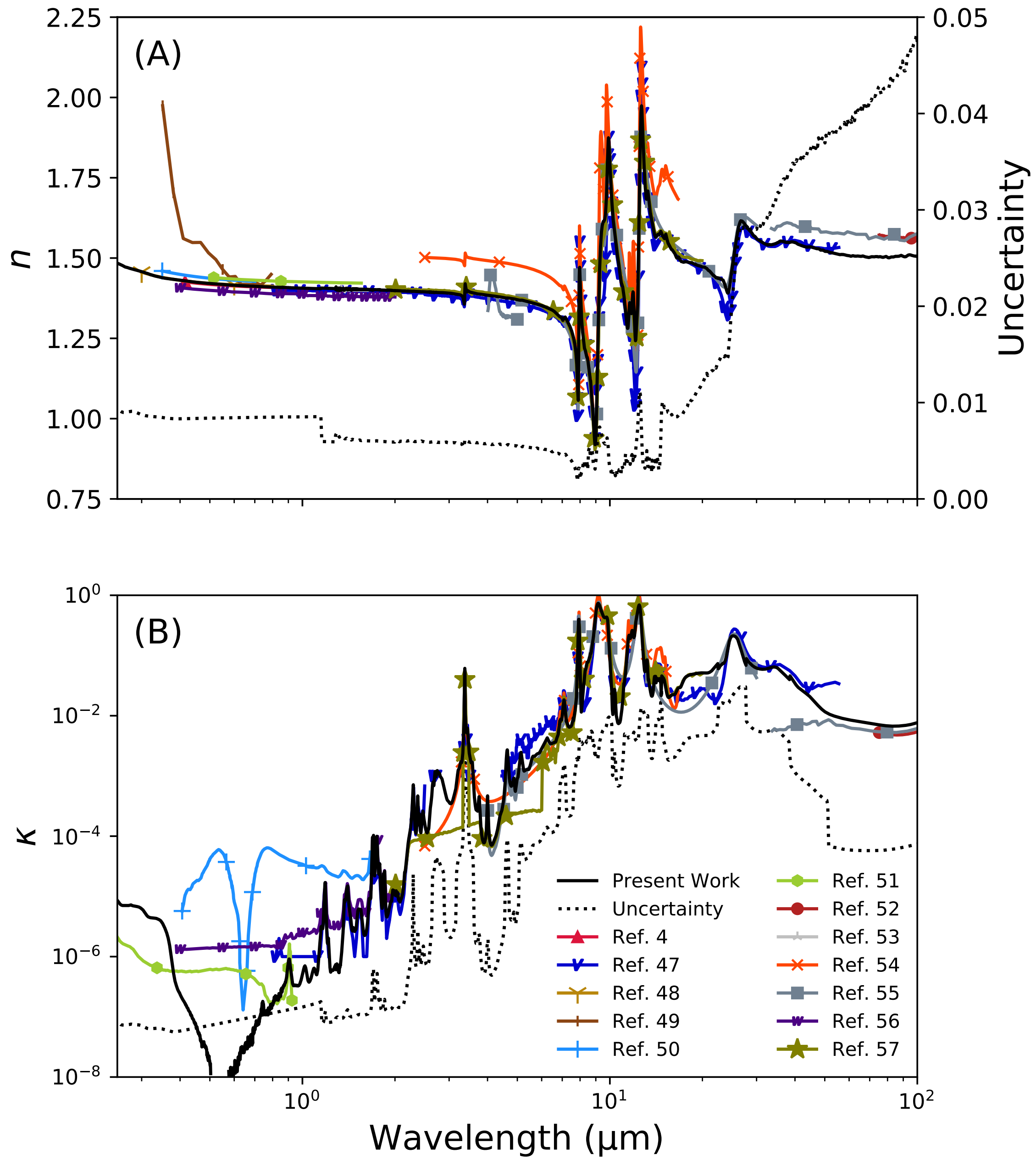

Fig 3 (A) Real part of complex refractive index from various works. The result of the present work and its $k = 2$ expanded uncertainty are shown with the solid and dashed black lines, respectively. (B) Imaginary part of complex refractive index from various works. The result of the present work and its $k = 2$ expanded uncertainty are shown with the solid and dashed black lines, respectively. The legend in (B) is common to both plots.

properties of the cooler and is given by

$$P_{\text{emit}}(T) = \int_0^\infty \pi L_{BB}(T) \left[2 \int_0^{\pi/2} \sin\theta \cos\theta \varepsilon(\theta, \lambda) d\theta \right] d\lambda \tag{14}$$

where T is the temperature of the radiative cooler, $L_{BB} = 2hc^2\lambda^{-5}(\exp(hc/\lambda k_B T) - 1)^{-1}$ is the spectral radiance of a blackbody, h is the Planck constant, k_B the Boltzmann constant, and ε is the spectral direction-hemispherical emittance of the radiative cooler at angle θ. θ is defined in relation to the surface normal of the radiative cooler.[7]

We examine the case of a $100\,\mu\text{m}$ thick layer of PDMS deposited on an aluminum substrate at $288\,\text{K}$. This structure was previously examined in Ref. 9. The radiative cooler was assumed to be a non-transmitting specular reflector with $\varepsilon(\theta, \lambda) = 1 - \frac{1}{2}[r_s(\theta, \lambda) + r_p(\theta, \lambda)]$, where r_s and r_p are the s- and p-polarization Fresnel reflection coefficients of the layered structure (computed using the transfer matrix method[58]). The reflection coefficients were computed using the complex refractive indices of PDMS from this work and aluminum from a Brendel–Bormann model[59] as inputs. Reference 59 did not provide uncertainty data so the uncertainty of the spectral emissive power was obtained by a Monte Carlo simulation which only accounted for the uncertainty in the optical properties of PDMS.

The spectral emissive power (integrand of Eq. 14) of the PDMS passive radiative cooler and a blackbody are shown in Fig. 4. The $k = 2$ expanded uncertainty of the spectral emissive power of the PDMS passive radiative cooler is shown in the inset. Numerically integrating the curves shown in Fig. 4, we predict an emissive power of $388.04\,\text{W/m}^2$ for the blackbody. That corresponds to $99.5\,\%$ of the emissive power predicted by the Stefan-Boltzmann law. Turning attention to the PDMS passive radiative cooler, we predict an emissive power of $(330.27 \pm 0.13)\,\text{W/m}^2$ ($k = 2$

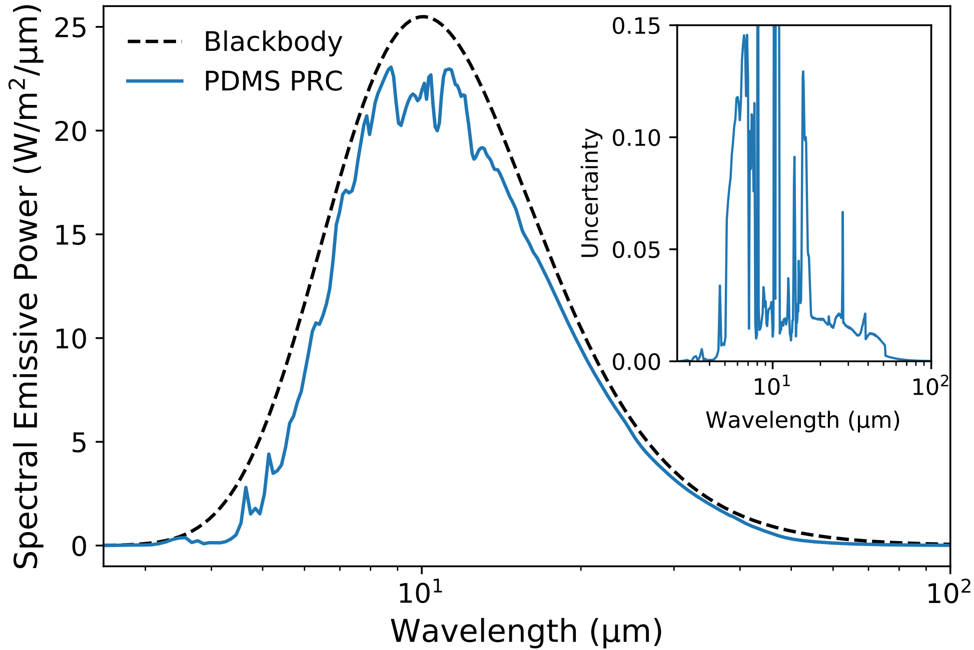

Fig 4 Spectral emissive power of a blackbody (dashed curve) and PDMS passive radiative cooler (solid curve). Inset: $k = 2$ expanded uncertainty.

expanded uncertainty). If instead we had access only to data out to the mid-infrared wavelength of $\lambda = 25\,\mu\text{m}$, we would predict an emissive power of $(278.09 \pm 0.13)\ \text{W}/\text{m}^2$. One natural method of extrapolating limited spectral data would be to assume the radiative cooler's emittance is constant at longer wavelengths, taking the value and uncertainty at $25\,\mu\text{m}$. Using that strategy, we would predict an emissive power of $(339.89 \pm 0.13)\ \text{W}/\text{m}^2$. The wide range of these estimates demonstrates that far infrared optical properties are crucial for an accurate prediction of radiative heat transfer of passive radiative coolers.

5 Conclusion

We implemented an algorithm for determining the complex refractive index of a material over a broad spectral range from spectrophotometric measurements. We validated the algorithm by computing the complex refractive index of PDMS between $0.25\,\mu\text{m}$ and $100\,\mu\text{m}$ and comparing

the results against existing literature, providing evidence that the algorithm is a powerful tool for analyzing commonly measured reflectance and transmittance measurements. While our results are similar to the existing literature for most wavelengths, we are the first to present continuous, broadband properties of PDMS with uncertainties which are well-suited to passive radiative calculations. Further, we demonstrated that broadband optical properties such as ours are necessary to accurately predict the performance of passive radiative cooling devices.

Future work on this algorithm should determine the conditions for the optimal locations of ω_{lower} and ω_{upper}, determine the best integration algorithm for computing $\beta(\omega)$, examine further the approximation as constants for $C_\alpha(\omega)$ and $C_\beta(\omega)$, and, if necessary, develop better approximations. Future work on the optical properties of PDMS should measure κ at visible wavelengths and investigate the differences between works to determine if they result from true material property differences or weaknesses in the measurements and analyses.

Disclosures

Portions of this work have previously appeared in SPIE Reflection, Scattering, and Diffraction from Surfaces VII conference proceedings.[60] The authors declare no conflicts of interest.

Acknowledgements

The authors would like to thank Dr. Catherine Cooksey for her instruction on operating the NIST transfer spectrophotometer and scheduling time to use the instrument. The authors would like to thank Dr. Simon Kaplan for his suggestion of using the V/W absolute reflection accessory in a relative configuration.

Appendix A: Uncertainty analysis

A.1 Nichelatti's Method

Starting from the measurement equations

$$\kappa = \frac{\lambda}{4\pi h} \ln\left(\frac{R_{12}T_{123}}{R_{123}-R_{12}}\right) \tag{1 revisited}$$

$$n = \frac{1+R_{12}}{1-R_{12}} + \sqrt{\left(\frac{1+R_{12}}{1-R_{12}}\right)^2 - 1 - \kappa^2}\,, \tag{2 revisited}$$

$$R_{12} = \frac{2+T_{123}^2-(1-R_{123})^2-\sqrt{(2+T_{123}^2-(1-R_{123})^2)^2-4R_{123}(2-R_{123})}}{2(2-R_{123})}\,, \tag{3 revisited}$$

$$R_{123} = \frac{(R_{12}^2+2R_{12}-1)+\sqrt{(2R_{12}T_{123})^2+(1-R_{12})^4}}{2R_{12}}\,, \tag{4 revisited}$$

we can write the Taylor approximation for uncorrelated parameters as

$$u\left(R_{123}\right) = \sqrt{\left(\frac{\partial R_{123}}{\partial R_{12}}\right)^2 u^2\left(R_{12}\right) + \left(\frac{\partial R_{123}}{\partial T_{123}}\right)^2 u^2\left(T_{123}\right)} \tag{15}$$

$$u\left(R_{12}\right) = \sqrt{\left(\frac{\partial R_{12}}{\partial R_{123}}\right)^2 u^2\left(R_{123}\right) + \left(\frac{\partial R_{12}}{\partial T_{123}}\right)^2 u^2\left(T_{123}\right)} \tag{16}$$

$$u\left(\kappa\right) = \sqrt{\left(\frac{\partial \kappa}{\partial R_{123}}\right)^2 u^2\left(R_{123}\right) + \left(\frac{\partial \kappa}{\partial T_{123}}\right)^2 u^2\left(T_{123}\right) + \left(\frac{\partial \kappa}{\partial h}\right)^2 u^2\left(h\right) + \left(\frac{\partial \kappa}{\partial \lambda}\right)^2 u^2\left(\lambda\right)} \tag{17}$$

$$u\left(n\right) = \sqrt{\left(\frac{\partial n}{\partial R_{123}}\right)^2 u^2\left(R_{123}\right) + \left(\frac{\partial n}{\partial T_{123}}\right)^2 u^2\left(T_{123}\right) + \left(\frac{\partial n}{\partial h}\right)^2 u^2\left(h\right) + \left(\frac{\partial n}{\partial \lambda}\right)^2 u^2\left(\lambda\right)}\,, \tag{18}$$

where $u(x)$ is the standard uncertainty of any variable x. Evaluating the partial derivatives in Eqs. (16)-(18), we get

$$\frac{1}{R_{12}}\frac{\partial R_{12}}{\partial R_{123}} = \frac{(1-R_{123})^3 + (1-R_{123})T_{123}^2 + \sqrt{(1-R_{123})^4 + 2(1+R_{123}(2-R_{123}))T_{123}^2 + T_{123}^4}}{R_{123}(2-R_{123})\sqrt{(1+T_{123}^2+R_{123}(2-R_{123}))^2 - 4R_{123}(2-R_{123})}} \tag{19}$$

$$\frac{1}{R_{12}}\frac{\partial R_{12}}{\partial T_{123}} = \frac{-2T_{123}}{\sqrt{(1+T_{123}^2+R_{123}(2-R_{123}))^2 - 4R_{123}(2-R_{123})}} \tag{20}$$

$$\frac{\partial \kappa}{\partial R_{123}} = \frac{\lambda}{4\pi h}\left(\frac{R_{123}\left(\frac{1}{R_{12}}\frac{\partial R_{12}}{\partial R_{123}}\right) - 1}{R_{123} - R_{12}}\right) \tag{21}$$

$$\frac{\partial \kappa}{\partial T_{123}} = \frac{\lambda}{4\pi h}\left(\frac{R_{123}\left(\frac{1}{R_{12}}\frac{\partial R_{12}}{\partial T_{123}}\right)T_{123} + (R_{123} - R_{12})}{(R_{123} - R_{12})\,T_{123}}\right) \tag{22}$$

$$\frac{\partial \kappa}{\partial h} = -\frac{\kappa}{h} \tag{23}$$

$$\frac{\partial \kappa}{\partial \lambda} = \frac{\kappa}{\lambda} \tag{24}$$

$$\frac{\partial n}{\partial R_{123}} = \left(\frac{2R_{12}}{(1-R_{12})^2}\right)\left(\frac{1}{R_{12}}\frac{\partial R_{12}}{\partial R_{123}}\right) + \frac{\left(\frac{1+R_{12}}{1-R_{12}}\right)\left(\frac{2R_{12}}{(1-R_{12})^2}\right)\left(\frac{1}{R_{12}}\frac{\partial R_{12}}{\partial R_{123}}\right) - \kappa\frac{\partial \kappa}{\partial R_{123}}}{\sqrt{2\left(\frac{2R_{12}}{(1-R_{12})^2}\right) - \kappa^2}} \tag{25}$$

$$\frac{\partial n}{\partial T_{123}} = \left(\frac{2R_{12}}{(1-R_{12})^2}\right)\left(\frac{1}{R_{12}}\frac{\partial R_{12}}{\partial T_{123}}\right) + \frac{\left(\frac{1+R_{12}}{1-R_{12}}\right)\left(\frac{2R_{12}}{(1-R_{12})^2}\right)\left(\frac{1}{R_{12}}\frac{\partial R_{12}}{\partial T_{123}}\right) - \kappa\frac{\partial \kappa}{\partial T_{123}}}{\sqrt{2\left(\frac{2R_{12}}{(1-R_{12})^2}\right) - \kappa^2}} \tag{26}$$

$$\frac{\partial n}{\partial h} = -\frac{\kappa\frac{\partial \kappa}{\partial h}}{\sqrt{2\left(\frac{2R_{12}}{(1-R_{12})^2}\right) - \kappa^2}} \tag{27}$$

$$\frac{\partial n}{\partial \lambda} = -\frac{\kappa\frac{\partial \kappa}{\partial \lambda}}{\sqrt{2\left(\frac{2R_{12}}{(1-R_{12})^2}\right) - \kappa^2}}\,. \tag{28}$$

A.2 Kramers-Kronig Analysis

The uncertainty of δ is dependent on the integration algorithm and the form of the integral used. i.e. using Eq. (6), Eq. (7), or some other equivalent integral. Here we will examine the propagation of the uncertainty of δ into values of n and κ.

Starting from the measurement equations

$$n = \frac{1 - R_{12}}{1 + R_{12} - 2\sqrt{R_{12}}\cos\delta} \tag{29}$$

$$\kappa = \frac{2\sqrt{R_{12}}\sin\delta}{1 + R_{12} - 2\sqrt{R_{12}}\cos\delta}\,, \tag{30}$$

we can write the Taylor approximation for uncorrelated parameters as

$$u\left(n\right) = \sqrt{\left(\frac{\partial n}{\partial R_{12}}\right)^2 u^2\left(R_{12}\right) + \left(\frac{\partial n}{\partial \delta}\right)^2 u^2\left(\delta\right)} \tag{31}$$

$$u\left(\kappa\right) = \sqrt{\left(\frac{\partial \kappa}{\partial R_{12}}\right)^2 u^2\left(R_{12}\right) + \left(\frac{\partial \kappa}{\partial \delta}\right)^2 u^2\left(\delta\right)}\,. \tag{32}$$

Evaluating the partial derivatives in Eqs. (31) and (32), we get

$$\frac{1}{n}\frac{\partial n}{\partial R_{12}} = \frac{(1 + R_{12})\cos\delta - 2\sqrt{R_{12}}}{\sqrt{R_{12}}(1 - R_{12})(1 + R_{12} - 2\sqrt{R_{12}}\cos\delta)} \tag{33}$$

$$\frac{1}{n}\frac{\partial n}{\partial \delta} = \frac{-2\sqrt{R_{12}}\sin\delta}{1 + R_{12} - 2\sqrt{R_{12}}\cos\delta} \tag{34}$$

$$\frac{1}{\kappa}\frac{\partial \kappa}{\partial R_{12}} = \frac{1 - R_{12}}{2R_{12}(1 + R_{12} - 2\sqrt{R_{12}}\cos\delta)} \tag{35}$$

$$\frac{1}{\kappa}\frac{\partial \kappa}{\partial \delta} = \frac{(1 + R_{12})\cos\delta - 2\sqrt{R_{12}}}{\sin\delta(1 + R_{12} - 2\sqrt{R_{12}}\cos\delta)}\,. \tag{36}$$

The explicit uncertainty formulas for n and κ reveal a weakness of the Kramers-Kronig ap-

proach: it can amplify uncertainty of the measurands. For weakly absorbing materials (small κ which implies small δ), the relative standard uncertainty of κ, $u(\kappa)/\kappa$, grows to infinity. For the same case, the relative standard uncertainty of n can actually reduce that of R_{12}. For $\delta \rightarrow 0$, $u(n)/n = [\sqrt{R_{12}}/(1 - R_{12})][u(R_{12})/R_{12}]$. Therefore the relative standard error of n will be less than that of R_{12} for all values of R_{12} less than $3/2 - \sqrt{5}/2 \approx 0.38$. That corresponds to highly transparent materials with refractive indices less than approximately 4.24.

Appendix B: Additional data

Here we provide data from intermediate steps of Algorithm 1, described in Sec. 2.3. These data are provided to assist readers in troubleshooting readers' implementations of the algorithm and reproducing the results of this work.

In Fig. 5, R_{123} was measured on the NIST transfer spectrophotometer and in the NIST Fourier transform infrared spectrophotometry facility on a custom integrating sphere. The data are merged into a single spectrum spanning between approximately $0.25\,\mu\text{m}$ and $18\,\mu\text{m}$ (orange curves with square markers). T_{123} was measured similarly in that spectral range, and extended to $100\,\mu\text{m}$ using a commercial Fourier transform infrared spectrophotometer capable of making measurements under vacuum (blue curve without markers).

Figure 6(A) shows the phase angle, δ, computed using Eqs. (8)-(13). Readers should note the values of α and γ [shown in Fig. 6(B)] are small but not insignificant contributions to δ.

Figure 7 shows the values of n and κ and their associated $k = 2$ expanded uncertainties obtained via Nichelatti's method and Kramers-Kronig analysis on the three planar samples and the wedged sample. Values of κ smaller than their expanded uncertainties or smaller than Kramers-Kronig analysis can discern are excluded to improve clarity of the figures.

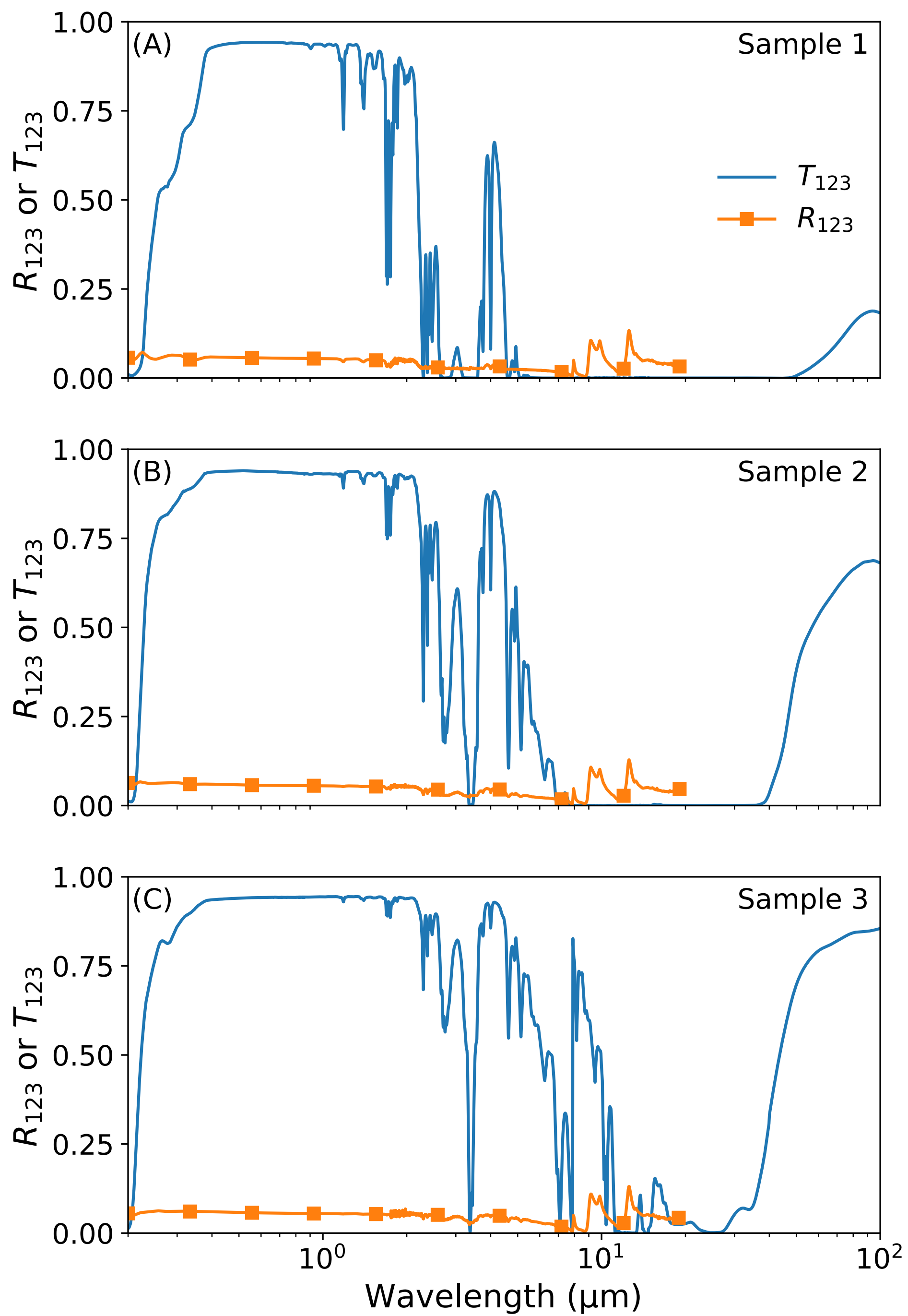

Fig 5 Measured values of R_{123} and T_{123} for (A) sample 1, (B) sample 2, and (C) sample 3. The legend in (A) is common to all plots.

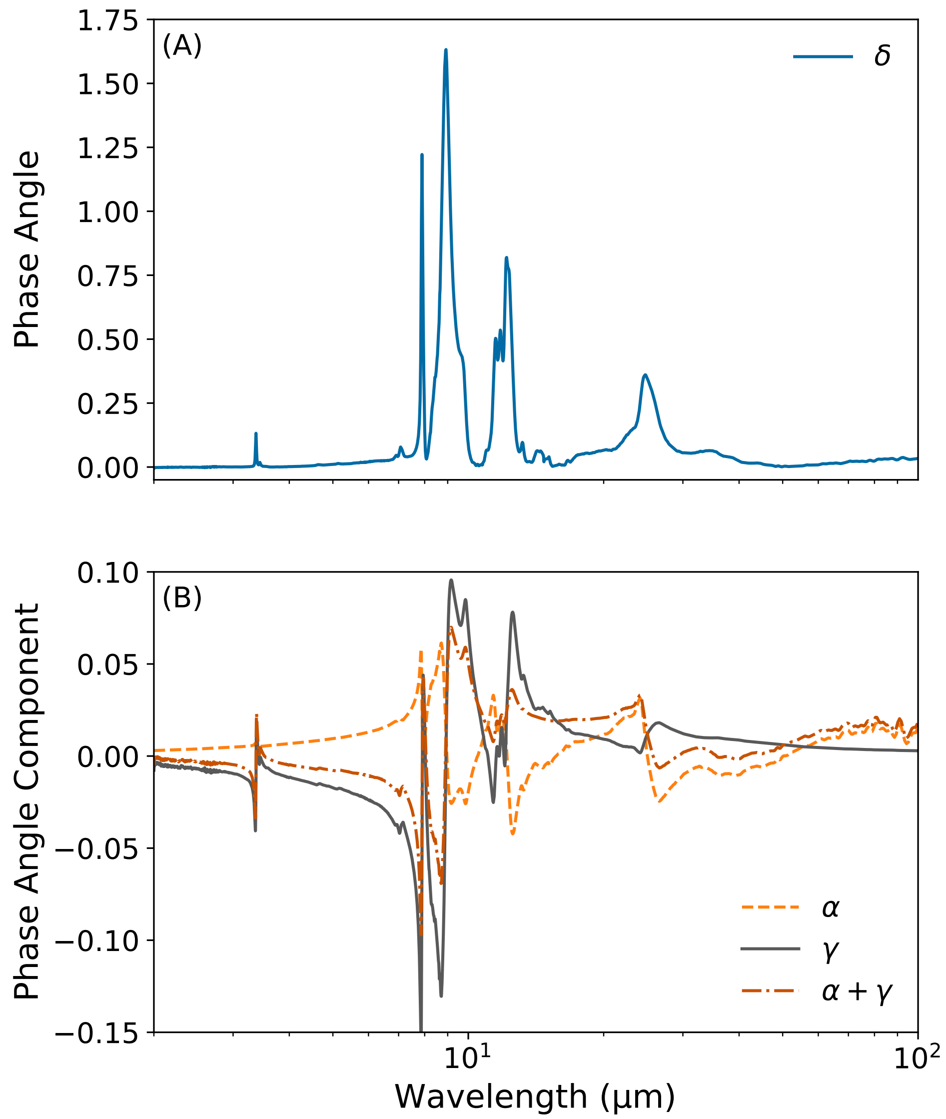

Fig 6 (A) Computed phase angle δ. (B) Components of phase angle computed from Eqs. (12) and (13).

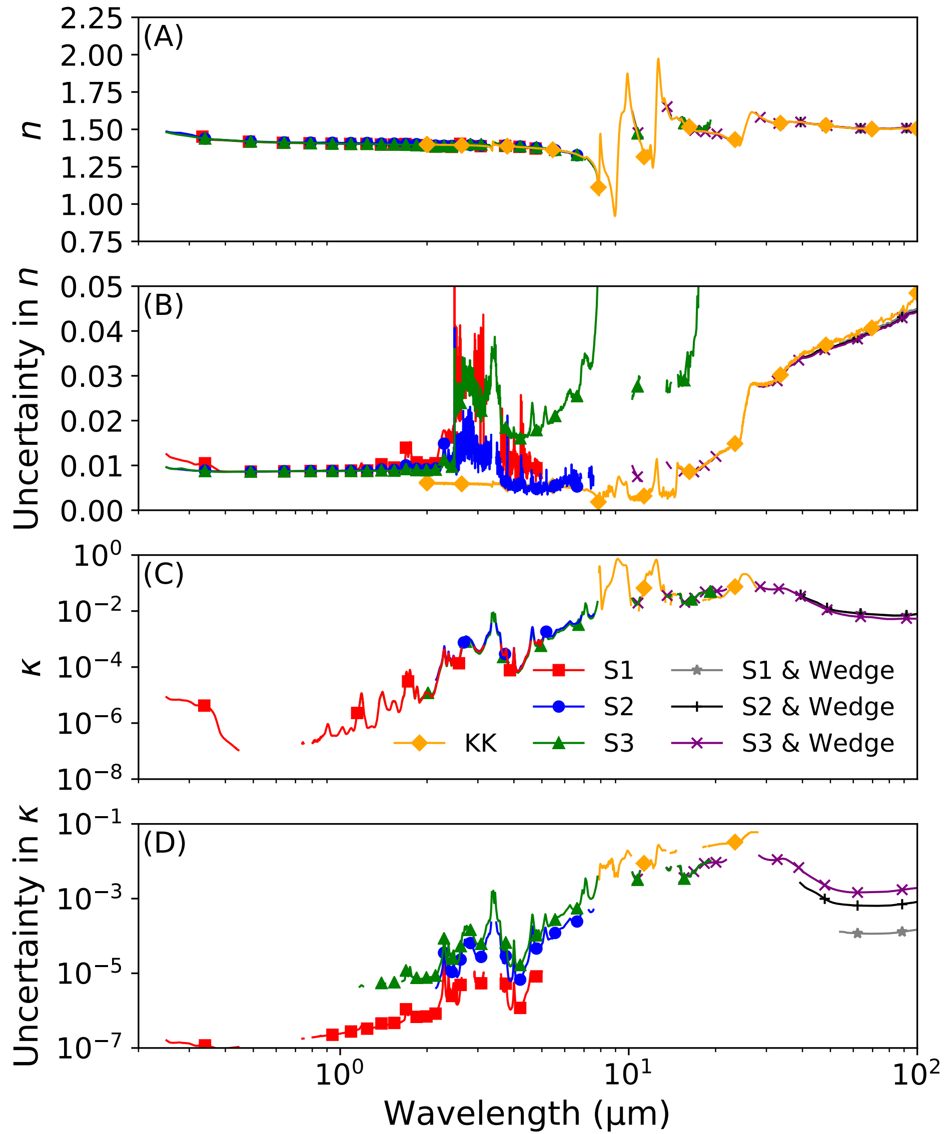

Fig 7 (A) All computed values of n. (B) Expanded ($k = 2$) uncertainties of values of n. (C) All computed values of κ. (D) Expanded ($k = 2$) uncertainties of κ. Legend in (C) is common to all plots. In the legend, curves 'S1,' 'S2,' and 'S3' refer to values computed by Nichelatti's method when R_{123} and T_{123} are measured on samples 1, 2, and 3, respectively. 'S1 & Wedge,' 'S2 & Wedge,' and 'S3 & Wedge' refer to values computed by Nichelatti's method when R_{12} and T_{123} are measured on samples 1, 2, and 3, respectively. 'KK' refers to values computed using Kramers-Kronig analysis.

References

1 W. M. Lee, A. Upadhya, P. J. Reece, *et al.*, "Fabricating low cost and high performance elastomer lenses using hanging droplets," *Biomedical Optics Express* **5**, 1626 (2014).

2 B. Dai, Z. Jiao, L. Zheng, *et al.*, "Colour compound lenses for a portable fluorescence microscope," *Light: Science & Applications* **8**, 75 (2019).

3 M. Kolle, B. Zheng, N. Gibbons, *et al.*, "Stretch-tuneable dielectric mirrors and optical microcavities," *Optics Express* **18**, 4356 (2010).

4 Z. Cai, W. Qiu, G. Shao, *et al.*, "A new fabrication method for all-PDMS waveguides," *Sensors and Actuators A: Physical* **204**, 44–47 (2013).

5 J. Guo, M. Niu, and C. Yang, "Highly flexible and stretchable optical strain sensing for human motion detection," *Optica* **4**, 1285 (2017).

6 A. Llobera, S. Demming, H. N. Joensson, *et al.*, "Monolithic PDMS passband filters for fluorescence detection," *Lab on a Chip* **10**, 1987 (2010).

7 B. Czapla, A. Srinivasan, Q. Yin, *et al.*, "Potential for Passive Radiative Cooling by PDMS Selective Emitters," in *Proceedings of the ASME 2017 Summer Heat Transfer Conference*, V001T09A015, ASME, (Bellevue) (2017).

8 J.-l. Kou, Z. Jurado, Z. Chen, *et al.*, "Daytime Radiative Cooling Using Near-Black Infrared Emitters," *ACS Photonics* **4**, 626–630 (2017).

9 L. Zhou, H. Song, J. Liang, *et al.*, "A polydimethylsiloxane-coated metal structure for all-day radiative cooling," *Nature Sustainability* **2**, 718–724 (2019).

10 C. G. Granqvist and A. Hjortsberg, "Radiative cooling to low temperatures: General consid-

erations and application to selectively emitting SiO films," *Journal of Applied Physics* **52**, 4205–4220 (1981).

11 A. Raman, M. A. Anoma, L. Zhu, *et al.*, "Passive radiative cooling below ambient air temperature under direct sunlight," *Nature* **515**, 540–544 (2014).

12 H. W. Verleur, "Determination of optical constants from reflectance or transmittance measurements on bulk crystals or thin films," *Journal of the Optical Society of America* **58**(10), 1356–1364 (1968).

13 M. R. Querry, "Direct Solution of the Generalized Fresnel Reflectance Equations," *Journal of the Optical Society of America* **59**, 876 (1969).

14 D. M. Kolb, "Determination of the Optical Constants of Solids by Reflectance-Ratio Measurements at Non-Normal Incidence," *Journal of the Optical Society of America* **62**, 599 (1972).

15 R. F. Miller, L. S. Julien, and A. J. Taylor, "A new computational method of obtaining optical constants from reflectance ratio measurements," *Journal of Physics D: Applied Physics* **5**, 318 (1972).

16 R. F. Miller, W. Hasan, and L. S. Julien, "A general procedure for evaluating optical constants from functions of reflectance at two angles of incidence," *Journal of Physics D: Applied Physics* **7**, 309 (1974).

17 R. M. A. Azzam, "Explicit determination of the complex refractive index of an absorbing medium from reflectance measurements at and near normal incidence," *Journal of the Optical Society of America* **72**, 1439 (1982).

18 E. Vartiainen, K. E. Peiponen, and T. Asakura, “Maximum entropy model in reflection spectra analysis,” *Optics Communications* **89**, 37–40 (1992).

19 K. F. Palmer, M. Z. Williams, and B. A. Budde, “Multiply subtractive Kramers–Kronig analysis of optical data,” *Applied Optics* **37**, 2660 (1998).

20 A. B. Kuzmenko, “Kramers–Kronig constrained variational analysis of optical spectra,” *Review of Scientific Instruments* **76**, 083108 (2005).

21 W. R. Hunter, “Errors in using the Reflectance vs Angle of Incidence Method for Measuring Optical Constants,” *Journal of the Optical Society of America* **55**, 1197 (1965).

22 E. Nichelatti, “Complex refractive index of a slab from reflectance and transmittance: analytical solution,” *Journal of Optics A: Pure and Applied Optics* **4**, 306 (2002).

23 H. A. Kramers, “La diffusion de la lumière par les atomes,” in *Atti Congressi Internazionale Fisica da Luigi Volta (Transactions of Volta Centenary Congress in Physics)*, **2**, 545–557, (Como, Italy) (1927).

24 R. de Ludwig Kronig, “On the Theory of Dispersion of X-Rays,” *Journal of the Optical Society of America* **12**, 547 (1926).

25 J. Bechhoefer, “Kramers–Kronig, Bode, and the meaning of zero,” *American Journal of Physics* **79**, 1053–1059 (2011).

26 K.-E. Peiponen and J. J. Saarinen, “Generalized Kramers–Kronig relations in nonlinear optical- and THz-spectroscopy,” *Reports on Progress in Physics* **72**, 056401 (2009).

27 P. Grosse and V. Offermann, “Analysis of reflectance data using the Kramers-Kronig Relations,” *Applied Physics A Solids and Surfaces* **52**, 138–144 (1991).

28 K. Yamamoto and H. Ishida, “Optical theory applied to infrared spectroscopy,” *Vibrational Spectroscopy* **8**, 1–36 (1994).

29 M. Sharnoff, “Validity Conditions for the Kramers-Kronig Relations,” *American Journal of Physics* **32**, 40–44 (1964).

30 T. S. Robinson, “Optical Constants by Reflection,” *Proceedings of the Physical Society. Section B* **65**(11), 910 (1952).

31 G. Leveque, “Reflectivity extrapolations in Kramers-Kronig analysis,” *Journal of Physics C: Solid State Physics* **10**, 4877–4888 (1977).

32 D. M. Roessler, “Kramers-Kronig analysis of reflection data,” *British Journal of Applied Physics* **16**, 1119–1123 (1965).

33 D. M. Roessler, “Kramers-Kronig analysis of non-normal incidence reflection,” *British Journal of Applied Physics* **16**, 1359–1366 (1965).

34 D. M. Roessler, “Kramers-Kronig analysis of reflectance data: III. Approximations, with reference to sodium iodide,” *British Journal of Applied Physics* **17**, 1313–1317 (1966).

35 K. Yamamoto and A. Masui, “Complex Refractive Index Determination of Bulk Materials from Infrared Reflection Spectra,” *Applied Spectroscopy, Vol. 49, Issue 5, pp. 639-644* **49**, 639–644 (1995).

36 M. Gottlieb, “Optical Properties of Lithium Fluoride in the Infrared,” *Journal of the Optical Society of America* **50**, 343 (1960).

37 F. C. Jahoda, “Fundamental absorption of barium oxide from its reflectivity spectrum,” *Physical Review* **107**, 1261–1265 (1957).

38 D. G. Thomas and J. J. Hopfield, "Exciton Spectrum of Cadmium Sulfide," *Physical Review* **116**, 573–582 (1959).

39 W. G. Spitzer and D. A. Kleinman, "Infrared lattice bands of quartz," *Physical Review* **121**, 1324–1335 (1961).

40 G. Andermann, A. Caron, and D. A. Dows, "Kramers-Kronig Dispersion Analysis of Infrared Reflectance Bands," *Journal of the Optical Society of America* **55**, 1210 (1965).

41 O. Stenzel, *The Physics of Thin Film Optical Spectra*, vol. 44 of *Springer Series in Surface Sciences*, Springer-Verlag, Berlin/Heidelberg (2005).

42 L. M. Hanssen, S. G. Kaplan, and R. Datla, "Infrared optical properties of materials," *NIST Special Publication* **250-94** (2015).

43 L. M. Hanssen and S. Kaplan, "Infrared diffuse reflectance instrumentation and standards at NIST," *Analytica Chimica Acta* **380**, 289–302 (1999).

44 L. M. Hanssen and K. A. Snail, "Integrating spheres for mid- and near infrared reflection spectroscopy," in *Handbook of Vibrational Spectroscopy*, J. M. Chalmers and P. R. Griffiths, Eds., 1175–1192, John Wiley & Sons, Ltd (2002).

45 L. M. Hanssen, A. V. Prokhorov, and V. B. Khromchenko, "Specular baffle for improved infrared integrating sphere performance," in *Optical Diagnostic Methods for Inorganic Materials III*, L. M. Hanssen, Ed., **5192**, 101, SPIE (2003).

46 L. M. Hanssen, "Integrating-sphere system and method for absolute measurement of transmittance, reflectance, and absorptance of specular samples," *Applied Optics* **40**, 3196 (2001).

47 M. R. Querry, "Optical Constants of Minerals and Other Materials from the Millimeter to the Ultraviolet," tech. rep., Chemical Research, Development & Engineering Center (1987).

48 K. Spaeth, G. Kraus, and G. Gauglitz, “In-situ characterization of thin polymer films for applications in chemical sensing of volatile organic compounds by spectroscopic ellipsometry,” *Fresenius Journal of Analytical Chemistry* **357**, 292–296 (1997).

49 A. M. Cardenas-Valencia, D. Fries, J. Dlutowski, *et al.*, “Spectrometric Determination of the Refractive Index of Optical Wave Guiding Materials Used in Lab-On-a-Chip Applications,” *Applied Spectroscopy, Vol. 60, Issue 3, pp. 322-329* **60**, 322–329 (2006).

50 F. Schneider, J. Draheim, R. Kamberger, *et al.*, “Process and material properties of polydimethylsiloxane (PDMS) for Optical MEMS,” *Sensors and Actuators A: Physical* **151**, 95–99 (2009).

51 D. Cai, A. Neyer, R. Kuckuk, *et al.*, “Raman, mid-infrared, near-infrared and ultraviolet–visible spectroscopy of PDMS silicone rubber for characterization of polymer optical waveguide materials,” *Journal of Molecular Structure* **976**, 274–281 (2010).

52 A. Podzorov and G. Gallot, “Density of states and vibrational modes of PDMS studied by terahertz time-domain spectroscopy,” *Chemical Physics Letters* **495**, 46–49 (2010).

53 D. Kacik, P. Tatar, and I. Martincek, “Measurement of PDMS refractive index by low-coherence interferometry,” in *2014 ELEKTRO*, 662–665, IEEE (2014).

54 A. Srinivasan, B. Czapla, J. Mayo, *et al.*, “Infrared dielectric function of polydimethylsiloxane and selective emission behavior,” *Applied Physics Letters* **109**, 061905 (2016).

55 E. Motaharifar, R. G. Pierce, R. Islam, *et al.*, “Broadband Terahertz Refraction Index Dispersion and Loss of Polymeric Dielectric Substrate and Packaging Materials,” *Journal of Infrared, Millimeter, and Terahertz Waves* **39**, 93–104 (2018).

56 X. Zhang, J. Qiu, X. Li, *et al.*, "Complex refractive indices measurements of polymers in visible and near-infrared bands," *Applied Optics* **59**, 2337 (2020).

57 X. Zhang, J. Qiu, J. Zhao, *et al.*, "Complex refractive indices measurements of polymers in infrared bands," *Journal of Quantitative Spectroscopy and Radiative Transfer* **252**, 107063 (2020).

58 S. J. Byrnes, "Multilayer optical calculations," *arXiv preprint arXiv:1603.02720* (2016).

59 A. D. Rakić, A. B. Djurišić, J. M. Elazar, *et al.*, "Optical properties of metallic films for vertical-cavity optoelectronic devices," *Applied Optics* **37**, 5271 (1998).

60 B. Czapla and L. M. Hanssen, "Direct method of extracting complex refractive index from routine Fourier transform infrared reflectance/transmittance measurements," in *Reflection, Scattering, and Diffraction from Surfaces VII*, L. M. Hanssen, Ed., **11485**, 11, SPIE (2020).

Braden Czapla is a mechanical engineer at the National Institute of Standards and Technology, where he researches how the measurement uncertainty in dimensional metrology is impacted by the optical properties of measured objects. His broader interests include radiative heat transfer, particularly radiative cooling and near-field radiative heat transfer, and spectrophotometry, predominantly at infrared wavelengths. He received a Ph.D. in mechanical engineering from Columbia University in 2019.

Leonard Hanssen is a physicist at the National Institute of Standards and Technology, where he is the project leader for the Infrared Optical Properties of Materials Program. His interests include the spectral infrared characterization of the optical and radiometric properties of materials, sources, and detectors, as well as the development of measurement methods and instrumentation,

especially integrating spheres, and standards. He received a Ph.D. in experimental physics from Cornell University in 1985.